*quantum beam science*

MDPI

*Article*

# Generalized N-Dimensional Effective Temperature for Cryogenic Systems in Accelerator Physics

**Heetae Kim [1,*] and Chang-Soo Park [2,*]**

[1] Institute for Rare Isotope Science, Institute for Basic Science, Daejeon 34000, Republic of Korea
[2] Quantum-Functional Semiconductor Research Center, Dongguk University, Seoul 04620, Republic of Korea
* Correspondence: kimht7@ibs.re.kr (H.K.); cspark@dongguk.edu (C.-S.P.)

**Abstract:** Investigations into the properties of generalized effective temperature are conducted across arbitrary dimensions. Maxwell–Boltzmann distribution is displayed for one, two, and three dimensions, with effective temperatures expressed for each dimension. The energy density of blackbody radiation is examined as a function of dimensionality. Effective temperatures for non-uniform temperature distributions in one, two, three, and higher dimensions are presented, with generalizations extended to arbitrary dimensions. Furthermore, the application of generalized effective temperature is explored not only for linearly non-uniform temperature distributions but also for scenarios involving the volume fraction of two distinct temperature distributions. The effective temperature is determined for a cryogenic system supplied with both liquid nitrogen and liquid helium. This effective temperature is applied to the Coefficient of Performance (COP) in cryogenic systems and can also be applied to high-energy accelerator physics, including high-dimensional physics.

**Keywords:** effective temperature; fractional dimension; thermal radiation; cryogenic system; accelerator physics



**Citation:** Kim, H.; Park, C.-S. Generalized N-Dimensional Effective Temperature for Cryogenic Systems in Accelerator Physics. *Quantum Beam Sci.* **2024**, *8*, 21. https://doi.org/10.3390/qubs8030021

Academic Editor: Andrew Stevenson

Received: 1 July 2024
Revised: 4 August 2024
Accepted: 21 August 2024
Published: 27 August 2024



## 1. Introduction

The temperature of a body is commonly assessed through the utilization of blackbody radiation. The exploration of Stefan–Boltzmann's law in n-dimensional space has been pursued [1]. It has been observed that thermal radiation exhibits notable deviations from blackbody radiation when considering bodies of a small size. Investigations into the size effect of thermal radiation in one, two, and three dimensions have been conducted [2–4]. Techniques for correcting camera and infrared detector errors have been developed to enhance temperature measurement accuracy [5–8], while investigations into minimum resolvable temperature have been conducted in the realm of thermal imaging sensing [9]. Furthermore, calculations of effective temperature for non-uniform temperature distributions have been investigated [10,11]. Additionally, research across various fields has delved into the fractal dimensions of natural phenomena and their applications [12–17]. Integer dimensions are idealized constructs, whereas fractional dimensions manifest in natural phenomena. The evaluation of fractal dimensions on the thermal and hydrodynamic properties of micro-channel rough surface structures was conducted using computational fluid dynamic simulations [18]. The heat capacity of liquid helium, which exhibits a fractal dimension between two and three dimensions, was calculated. The results showed a significant dependence on this fractal dimension [19]. The fractional dimension of a body can be discerned through the measurement of the maximum frequency of thermal radiation. A study explored how the most probable frequency of emitted radiation relates to thermal energy across arbitrary dimensions [20]. Furthermore, the study of temperature-independent thermal radiation—where the color remains constant despite temperature variations—was investigated through insulator-to-metal phase transitions [21]. To construct high-energy accelerators, superconducting cavities are essential for accelerating high-energy beams.

Cryogenic systems were constructed, superconducting cavities were developed, and the surface resistance of these cavities was investigated [22–25]. The temperature of cryogenic systems is important, and the effective temperature can be useful for regions with non-uniform temperatures. The effective temperature of a cryogenic system is crucial, as it directly influences the cooling temperature of the body and the volume of the cryogenic system, particularly when using liquid helium and liquid nitrogen. These factors are closely tied to the overall cost of the system.

In this study, we investigate the properties of generalized effective temperature across arbitrary dimensions. We examine the energy density of blackbody radiation in relation to dimensionality. Generalized effective temperatures for non-uniform temperature distributions are derived for one, two, and three dimensions, with extensions to fractional dimensions and arbitrary higher dimensions. We explore the effective temperature for linearly non-uniform temperature distributions across arbitrary dimensions, as well as its variation with volume fraction. Additionally, we estimate the effective temperature when a low-temperature test system is supplied with liquid nitrogen and liquid helium.

## 2. Maxwell–Boltzmann Distribution for One, Two, and Three Dimensions

The one-dimensional Maxwell–Boltzmann distribution for a gas is given by

$$f(v_x) = (\frac{m}{2\pi k_B T})^{1/2} e^{-mv_x^2/2k_B T}, \tag{1}$$

where $v_x$ is the velocity in x-direction and m is the mass of the particles. For a one-dimensional velocity distribution, the most probable velocity is $v_{mp} = 0$, the average velocity is $v_{av} = \sqrt{\frac{2k_B T}{m}}$, and the root-mean-square velocity is $v_{rms} = \sqrt{\frac{k_B T}{m}}$.

The velocity distribution for two different temperature regions in one dimension is given by

$$f(v_x) = (\frac{n_1}{n_1+n_2})(\frac{m}{2\pi k_B T_1})^{1/2} e^{-\frac{mv_x^2}{2k_B T_1}} + \left(\frac{n_2}{n_1+n_2}\right)\left(\frac{m}{2\pi k_B T_2}\right)^{1/2} e^{-\frac{mv_x^2}{2k_B T_2}}, \tag{2}$$

where $n_1$ is the number of particles in the temperature $T_1$ region and $n_2$ is the number of particles in the temperature $T_2$ region.

The effective temperature for the two different temperature distributions is

$$T_{eff} = [(\frac{n_1}{n_1+n_2})T_1^2 + (\frac{n_2}{n_1+n_2})T_2^2]^{1/2}. \tag{3}$$

The velocity distribution in terms of the effective temperature in one dimension is

$$f(v) = (\frac{m}{2\pi k_B T_{eff}})^{1/2} e^{-mv_x^2/2k_B T_{eff}}. \tag{4}$$

The two-dimensional Maxwell–Boltzmann distribution is given by

$$f(v) = (\frac{m}{2\pi k_B T}) e^{-m(v_x^2+v_y^2)/2k_B T}, \tag{5}$$

where $v^2 = v_x^2 + v_y^2$. For a two-dimensional velocity distribution, the most probable velocity is $v_{mp} = \sqrt{\frac{k_B T}{m}}$, the average velocity is $v_{av} = \sqrt{\frac{\pi k_B T}{2m}}$, and the root-mean-square velocity is $v_{rms} = \sqrt{\frac{2k_B T}{m}}$.

The velocity distribution for two different temperature regions in two dimensions is

$$f(v) = (\frac{n_1}{n_1+n_2})(\frac{m}{2\pi k_B T_1})^{2/2} e^{-m(v_x^2+v_y^2)/2k_B T_1} + (\frac{n_2}{n_1+n_2})(\frac{m}{2\pi k_B T_2})^{2/2} e^{-m(v_x^2+v_y^2)/2k_B T_2}, \tag{6}$$

where $n_1$ is the number of particles in the temperature $T_1$ region and $n_2$ is the number of particles in the temperature $T_2$ region.

The effective temperature for the two different temperature distributions in two dimensions is

$$T_{eff} = [(\frac{n_1}{n_1+n_2})T_1^3 + (\frac{n_2}{n_1+n_2})T_2^3]^{1/3}. \quad (7)$$

The velocity distribution in terms of the effective temperature in two dimensions is

$$f(v) = (\frac{m}{2\pi k_B T_{eff}})e^{-m(v_x^2+v_y^2)/2k_B T_{eff}}. \quad (8)$$

The three-dimensional Maxwell–Boltzmann distribution is given by

$$f(v) = (\frac{m}{2\pi k_B T_{eff}})^{3/2} e^{-m(v_x^2+v_y^2+v_z^2)/2k_B T}, \quad (9)$$

where $v^2 = v_x^2 + v_y^2 + v_z^2$. For a three-dimensional velocity distribution, the most probable velocity is $v_{mp} = \sqrt{\frac{2k_B T}{m}}$, the average velocity is $v_{av} = \sqrt{\frac{8k_B T}{\pi m}}$, and the root-mean-square velocity is $v_{rms} = \sqrt{\frac{3k_B T}{m}}$.

The velocity distribution for two different temperature regions in three dimensions is

$$f(v) = (\frac{n_1}{n_1+n_2})(\frac{m}{2\pi k_B T_1})^{3/2} e^{-m(v_x^2+v_y^2+v_z^2)/2k_B T_1} + (\frac{n_2}{n_1+n_2})(\frac{m}{2\pi k_B T_2})^{3/2} e^{-m(v_x^2+v_y^2+v_z^2)/2k_B T_2}, \quad (10)$$

where $n_1$ is the number of particles in the temperature $T_1$ region and $n_2$ is the number of particles in the temperature $T_2$ region.

The effective temperature for the two different temperature distributions in three dimensions is

$$T_{eff} = [(\frac{n_1}{n_1+n_2})T_1^4 + (\frac{n_2}{n_1+n_2})T_2^4]^{1/4}. \quad (11)$$

The velocity distribution in terms of the effective temperature in three dimensions is

$$f(v) = (\frac{m}{2\pi k_B T_{eff}})^{3/2} e^{-m(v_x^2+v_y^2+v_z^2)/2k_B T_{eff}}. \quad (12)$$

## 3. Blackbody Radiation in Arbitrary Dimensions

While blackbody radiation in integer dimensions is well understood, we can extend this concept to arbitrary dimensions. For comparison, the energy density of one-dimensional blackbody radiation is given by [4]

$$u = (\frac{2\pi^2 k_B^2}{3hc})T^2, \quad (13)$$

where $k_B$ represents the Boltzmann constant, $T$ denotes the absolute temperature, $h$ stands for the Planck constant, and $c$ denotes the speed of light. The energy density of two-dimensional blackbody radiation becomes [3]

$$u_B(T) = 8\pi\zeta(3)\left[\frac{(k_B T)^3}{(hc)^2}\right], \quad (14)$$

where $\zeta$ stands for the Riemann zeta function. The energy density for blackbody radiation in three dimensions is [2]

$$u_B(T) = \left(\frac{8\pi^5}{15}\right)\left[\frac{(k_B T)^4}{(hc)^3}\right]. \quad (15)$$

The energy density in Equations (13)–(15) is proportional to the temperature raised to a power that reflects the total dimensionality. This total dimensionality includes both

spatial and temporal components. While the spatial dimension can be arbitrary, time is always one-dimensional.

Dimension, which includes integer dimension as well as fractional dimension, can be calculated as

$$D = \frac{\ln N}{\ln\left(\frac{1}{S}\right)}, \tag{16}$$

where $D$ is the dimension, $S$ is the scaling factor, and $N$ is the number of pieces. The dimension of an object can be determined using an arbitrary scaling factor. Equation (16) allows us to calculate the arbitrary dimension for any given geometry. Figure 1a shows one-dimension for $S = 1/5$ and $N = 5$, Figure 1b shows two-dimension for $S = 1/5$ and $N = 25$, and Figure 1c shows three-dimension for $S = 1/5$ and $N = 125$ by using Equation (16). A fractal has a non-integer dimension and exhibits self-similarity, meaning that a small part of the object resembles the entire object. Figure 1f represents $D = 1.062$ for $S = 1/12$ and $N = 14$, while Figure 1d,e show the process used to create Figure 1f. The surface area and the volume for arbitrary dimension in Euclidean space are $S_D(R) = \frac{2\pi^{(D+1)/2}}{\Gamma[(D+1)/2]} R^D$ and $V_D(R) = \frac{\pi^{D/2}}{\Gamma\left(\frac{D}{2}+1\right)} R^D$, respectively, in which $R$ means the radius of the Euclidean plane and $D$ means the dimension. Figure 1g,h refer to the surface area and the volume as a function of dimension for the radius of 1 m in Euclidean space. The volume and surface area of an object increase as the dimensions increase.

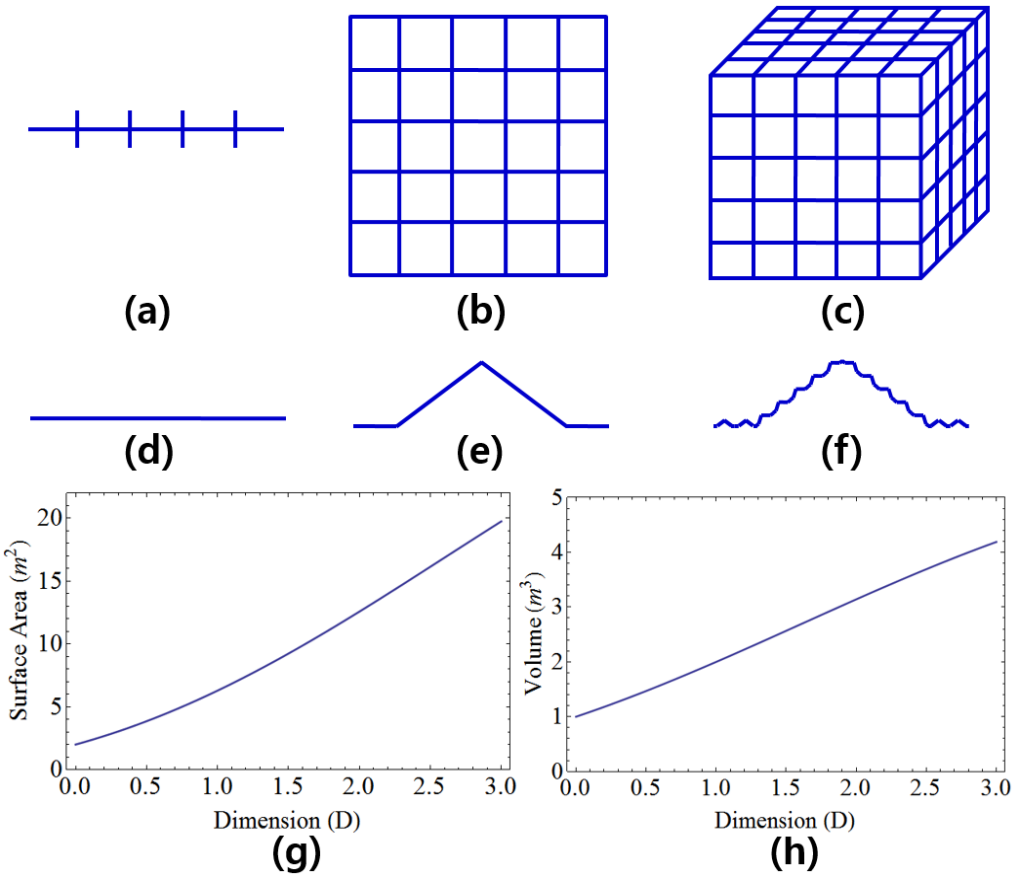


**Figure 1.** Integer and fractional dimensions: Subfigure (**a**) displays one dimension for $S = 1/5$ and $N = 5$, while subfigure (**b**) depicts two dimensions for $S = 1/5$ and $N = 25$. Subfigure (**c**) shows three dimensions for $S = 1/5$ and $N = 125$. Subfigures (**d**–**f**) illustrate $D = 1.062$ for $S = 1/12$ and $N = 14$. Subfigures (**g**,**h**) depict the surface area and volume as a function of dimension for a radius of 1 m in Euclidean space.

The energy density of the blackbody radiation in arbitrary dimensions is given by [1,20]

$$u_B(D,T) = \frac{4\pi^{D/2}\Gamma(D+1)\varsigma(D+1)}{\Gamma(D/2)}\left(\frac{(k_BT)^{D+1}}{(hc)^D}\right), \tag{17}$$

where $\Gamma$ is the gamma function and $D$ denotes the spatial dimension. The energy density increases with temperature as $T^{(D+1)}$, where $D$ represents the spatial dimension, and the additional power of one accounts for the time dimension.

## 4. Effective Temperature for One, Two, and Three Dimensions

The total energy density of one-dimensional thermal radiation is calculated as:

$$u = \left(\frac{2\pi^2k_B^2}{3hc}\right)T_{eff}^2, \tag{18}$$

Here, $T_{eff}$ represents the effective temperature of the entire body. For a one-dimensional blackbody with uniform temperature distribution, the effective temperature remains constant throughout the body. Using Equations (13) and (18), we can derive the effective temperatures for three different temperature distributions, denoted as $T_1$, $T_2$, and $T_3$,

$$T_{eff} = \left[\left(\frac{L_1}{L}\right)T_1^2 + \left(\frac{L_2}{L}\right)T_2^2 + \left(\frac{L_3}{L}\right)T_3^2\right]^{1/2}, \tag{19}$$

where $L$ represents the total length of the body, with $L_1$, $L_2$, and $L_3$ denoting the lengths corresponding to temperatures $T_1$, $T_2$, and $T_3$, respectively. It is important to note that the effective temperature of the body always surpasses the average temperature when dealing with more than two different temperature regions. For a one-dimensional non-uniform temperature distribution, the effective temperature of n segments can be generalized as

$$T_{eff} = \left[\left(\frac{1}{L}\right)\sum_{i=1}^{n} L_iT_i^2\right]^{1/2}, \tag{20}$$

where $L = \sum_{i=1}^{n} L_i$. The effective temperature is defined for discrete non-uniform temperature distribution in Equation (20). For continuously changing temperature distribution in one dimension, the effective temperature can be expressed as

$$T_{eff} = \sqrt[2]{\int \frac{T(l)^2}{L}dl}. \tag{21}$$

The total energy density of two-dimensional thermal radiation is calculated as

$$u = \left(\frac{8\pi\zeta(3)k_B^3}{(hc)^2}\right)T_{eff}^3, \tag{22}$$

where $T_{eff}$ represents the effective temperature across a two-dimensional body. Using Equations (14) and (22), we can calculate the effective temperatures for three different temperature distributions

$$T_{eff} = \left[\left(\frac{A_1}{A}\right)T_1^3 + \left(\frac{A_2}{A}\right)T_2^3 + \left(\frac{A_3}{A}\right)T_3^3\right]^{1/3}, \tag{23}$$

where $A$ represents the total surface area of the body, with $A_1$, $A_2$, and $A_3$ denoting the surface areas corresponding to temperatures $T_1$, $T_2$, and $T_3$, respectively. It is important to note that the average temperature is lower than the effective temperature for three different

temperatures. In two dimensions, the effective temperature for $n$ segments with varying temperature distributions can be generalized as

$$T_{eff} = \left[\frac{1}{A}\sum_{i=1}^{n} A_i T_i^3\right]^{1/3}, \tag{24}$$

where $A = \sum_{i=1}^{n} A_i$ represents the total surface area of the two-dimensional body. Equation (24) provides the definition of the effective temperature for discrete non-uniform temperature distribution in two dimensions. For continuously non-uniform temperature distribution in two dimensions, the effective temperature can be expressed as

$$T_{eff} = \sqrt[3]{\int \frac{T(a)^3}{A} da}. \tag{25}$$

The total energy density for thermal radiation in three dimensions is given by

$$u(T) = (\frac{8\pi^5 k_B^4}{15h^3c^3})T_{eff}^4, \tag{26}$$

where $T_{eff}$ represents the effective temperature across a three-dimensional body. From Equations (15) and (26), the effective temperature of a body with three different temperature distributions can be expressed as

$$T_{eff} = [(\frac{V_1}{V})T_1^4 + (\frac{V_2}{V})T_2^4 + (\frac{V_3}{V})T_3^4]^{1/4}, \tag{27}$$

where $V$ represents the total volume of the body, with $V_1$, $V_2$, and $V_3$ denoting the volumes corresponding to temperatures $T_1$, $T_2$, and $T_3$, respectively. The effective temperature of the body for the $n$ segments of different temperature distributions in three-dimensional thermal radiation can be generalized as

$$T_{eff} = [\frac{1}{V}\sum_{i=1}^{n} V_i T_i^4]^{1/4}, \tag{28}$$

where $V$ represents the total volume of the body, given by $V = \sum_{i=1}^{n} V_i$. The effective temperature is defined for discrete non-uniform three-dimensional temperature distribution in Equation (28), where many small bodies have different temperatures.

The effective temperature of continuously non-uniform temperature distribution in three dimensions is expressed as

$$T_{eff} = \sqrt[4]{\int \frac{T(v)^4}{V} dv}. \tag{29}$$

## 5. Effective Temperature for Arbitrary Dimension

Many natural physical systems exhibit fractional dimensions, which often deviate from regular geometric shapes. For instance, while a line is typically considered one-dimensional, the dimension of a curved line exceeds one dimension. Similarly, while a perfectly smooth surface is typically two-dimensional, the dimension of a surface with roughness surpasses two dimensions. This study investigates the thermal radiation properties across arbitrary dimensions, highlighting the correlation between maximum radiation frequency and these dimensions [20]. The factor, $factor(D) = h \cdot \nu_{\max}/k_B T$, where $h$ represents Planck's constant, $\nu_{\max}$ is the maximum frequency, and $T$ is the absolute temperature, depending on the dimensions. The factors for one, two, and three dimensions are 0, 1.59362, and 2.82144, respectively. The factors for 2.1, 2.2, and 2.3 dimensions are 1.72634, 1.85622, and 1.98357, respectively [20]. The actual dimension of the body can be measured by detecting the most probable frequency.

The total energy density of the thermal radiation for both fractional dimension and arbitrary dimension is given by

$$u(D,T) = [\frac{4\pi^{D/2}\Gamma(D+1)\varsigma(D+1)k_B^{D+1}}{\Gamma(D/2)h^D c^D}]T_{eff}^{D+1}, \tag{30}$$

Here, $h$ represents the Planck constant, $c$ denotes the speed of light, $D$ signifies the spatial dimension, and $T_{eff}$ stands for the effective temperature of the body.

Combining Equations (17) and (30), the effective temperature of a body with three different temperature distributions in D-dimension can be formulated as

$$T_{eff} = [(\frac{v_1}{v})T_1^{D+1} + (\frac{v_2}{v})T_2^{D+1} + (\frac{v_3}{v})T_3^{D+1}]^{1/(D+1)}, \tag{31}$$

Here, $v$ denotes the total volume of the body, while $v_1$, $v_2$, and $v_3$ represent the volumes corresponding to temperatures $T_1$, $T_2$, and $T_3$, respectively. For $n$ segments exhibiting different temperature distributions, the generalized effective temperature of the body in arbitrary-dimensional thermal radiation is given by

$$T_{eff} = [\frac{1}{v}\sum_{i=1}^{n} v_i T_i^{D+1}]^{1/(D+1)}, \tag{32}$$

where $v = \sum_{i=1}^{n} v_i$ and $D$ represents the spatial dimension. The generalized effective temperature of continuously changing temperature distribution in arbitrary D-dimension can be expressed as

$$T_{eff} = \sqrt[D+1]{\int \frac{T(v)^{D+1}}{v} dv}. \tag{33}$$

where $T_{eff}$ stands for the effective temperature of the body, $v$ denotes the total volume of the body, $T$ is the absolute temperature, and $D$ represents the spatial dimension. Equation (33) represents the most generalized effective temperature for continuously changing temperature distributions in D-dimension, applicable to both fractional and arbitrary dimensions. The effective temperature of a system can be determined from Equation (33) once the temperature distribution of the system is known or measured. Using Equation (33), the effective temperatures for one, two, and three dimensions can be derived as shown in Equation (21), Equation (25), and Equation (29), respectively.

## 6. Results and Discussion

The effective temperature of a cryogenic system is of utmost importance as it dictates the required cooling power and associated costs for achieving desired temperatures. Figure 2 depicts the cryogenic system designed for a quarter-wave resonator cryomodule, where the superconducting cavity is cooled using both liquid nitrogen and liquid helium. These cryogenic liquids, with boiling points at 77 K and 4.2 K, respectively, are widely employed in cryogenic applications due to their effectiveness in cooling systems.

Figure 3 illustrates the effective temperature of linearly non-uniform temperature distribution for both liquid nitrogen and liquid helium. It serves as a valuable reference when examining thermal contact from room temperature to cryogenic temperatures. The effective temperature of the system can be determined from the generalized effective temperature in Equation (33) once the temperature distribution of the system is known. Using Equation (33), the effective temperatures for one, two, and three dimensions can be derived as shown in Equation (21), Equation (25), and Equation (29), respectively.

The linearly non-uniform temperature distribution between liquid nitrogen and room temperature is given by $T(x) = 77 + (300 - 77)x/L$, where $x$ is the distance and $L$ represents the total length of the body. For the linearly non-uniform temperature distribution ranging from 77 K to 300 K, the effective temperatures for one, two, and three dimensions are 199.2 K, 208.3 K, and 216.0 K, respectively. The average temperature is calculated as 188.5 K.

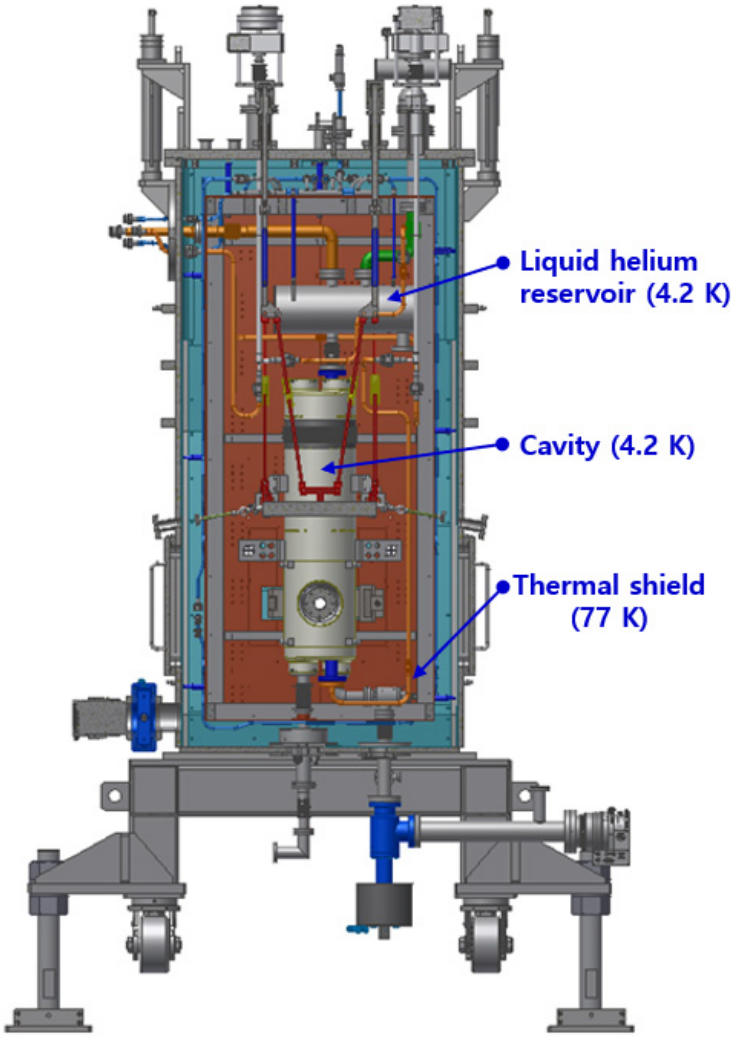


**Figure 2.** A cryogenic system for a quarter-wave resonator cryomodule. The superconducting cavity within the cryomodule is cooled using a combination of liquid nitrogen and liquid helium.

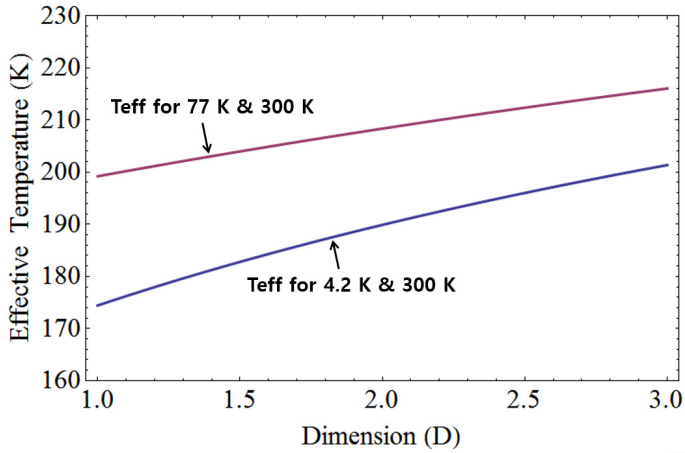


**Figure 3.** The effective temperature of a linearly non-uniform temperature distribution for both liquid nitrogen and liquid helium. In the top graph, the effective temperature ranges from 77 K to 300 K. For one, two, and three dimensions, the respective effective temperatures are 199.2 K, 208.3 K, and 216.0 K. The bottom graph displays the effective temperature ranging from 4.2 K to 300 K. In this range, the effective temperatures for one, two, and three dimensions are 174.4 K, 189.9 K, and 201.3 K, respectively.

Additionally, for the linearly non-uniform temperature between liquid helium and room temperature, the equation is given by $T(x) = 4.2 + (300 - 4.2)x/L$, where $x$ is the distance and $L$ represents the total length of the body. For the linearly non-uniform temperature distribution ranging from 4.2 K to 300 K, the effective temperatures for one, two, and three dimensions are 174.4 K, 189.9 K, and 201.3 K, respectively. These values are obtained using Equations (21), (25), and (29) to calculate the effective temperature for one, two, and three dimensions, respectively. Equations (21), (25), and (29) can be derived from the generalized effective temperature expression in Equation (33). The average temperature is determined to be 152.1 K. Notably, the effective temperature of a body exceeds its average temperature, and it increases with higher dimensions.

Figure 4 depicts the effective temperature with identical volume ratios for liquid helium and room temperature, as well as for liquid nitrogen and room temperature. In the top graph of Figure 4, the effective temperature is shown with the same volume ratio for 77 K and 300 K, while in the bottom graph, it is shown for 4.2 K and 300 K. It is observed that the effective temperature increases with higher dimensions. Furthermore, the disparity in effective temperature between the two cases decreases as the dimensionality is increased.

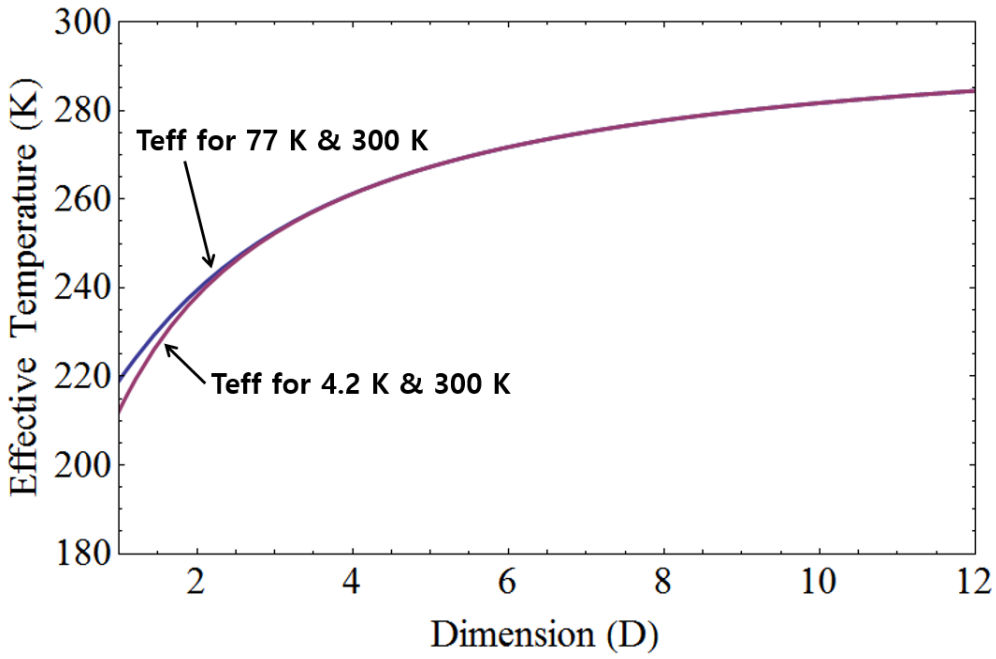


**Figure 4.** The effective temperature illustrated for liquid helium and room temperature, as well as for liquid nitrogen and room temperature, maintaining the same volume ratio. In the top graph, the effective temperature is plotted for 77 K and 300 K. Similarly, the bottom graph displays the effective temperature for 4.2 K and 300 K. Notably, the effective temperature shows an increase with higher dimensions.

In Figure 5, the effective temperature is presented as a function of the volume ratio for liquid helium and room temperature. The effective temperature is determined using the generalized effective temperature equation, Equation (33). Specifically, the graph illustrates the effective temperature with respect to the volume ratio of the 300 K volume to the 4.2 K volume. As anticipated, the effective temperature rises as the volume ratio increases. Moreover, it is noted that the effective temperature also escalates with increasing dimensionality while maintaining the same volume ratio. The effective temperature for $D = 3$ represents a cryogenic system and can be determined once the volume ratio of the 300 K volume to the 4.2 K volume is known. The effective temperature for $D = 2$ can be applied to two-dimensional materials such as graphene, while the effective temperature for $D = 1$ can be applied to one-dimensional materials such as carbon nanotubes.

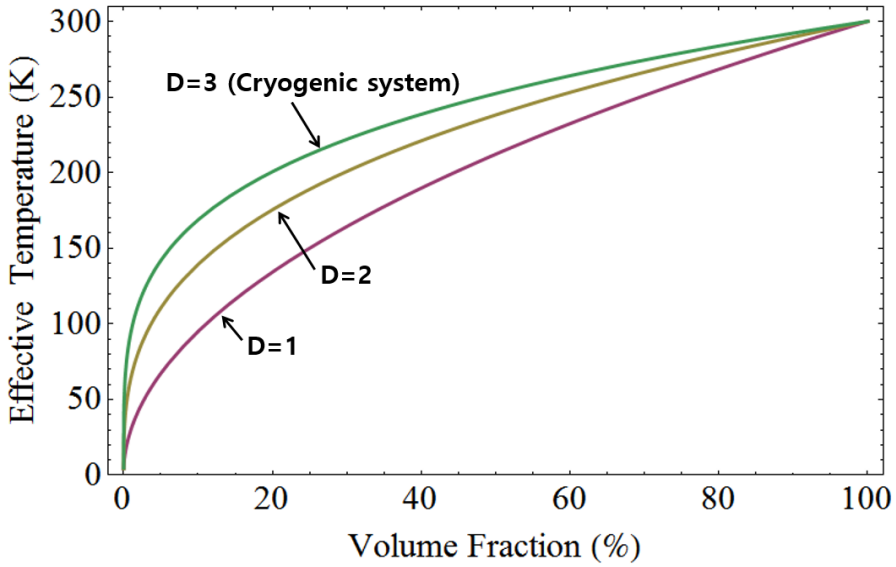


**Figure 5.** The effective temperature depicted as a function of the volume ratio for liquid helium and room temperature. Specifically, the effective temperature is presented with respect to the volume ratio of the 300 K volume to the 4.2 K volume. Notably, the effective temperature demonstrates an increase with higher dimensions or increased volume ratios.

Figure 6 illustrates the effective temperature as a function of the volume ratio, specifically the ratio of 300 K volume to 77 K volume. The generalized effective temperature equation, Equation (33), is used to determine the effective temperature of the system. It is evident that the effective temperature increases with both increasing dimensionality and volume ratio. The effective temperature for $D = 1$ can be applied to one-dimensional materials such as carbon nanotubes, while the effective temperature for $D = 2$ can be applied to two-dimensional materials such as graphene. The effective temperature for $D = 3$ represents a cryogenic system and can be determined once the volume ratio of the 300 K volume to the 77 K volume is known.

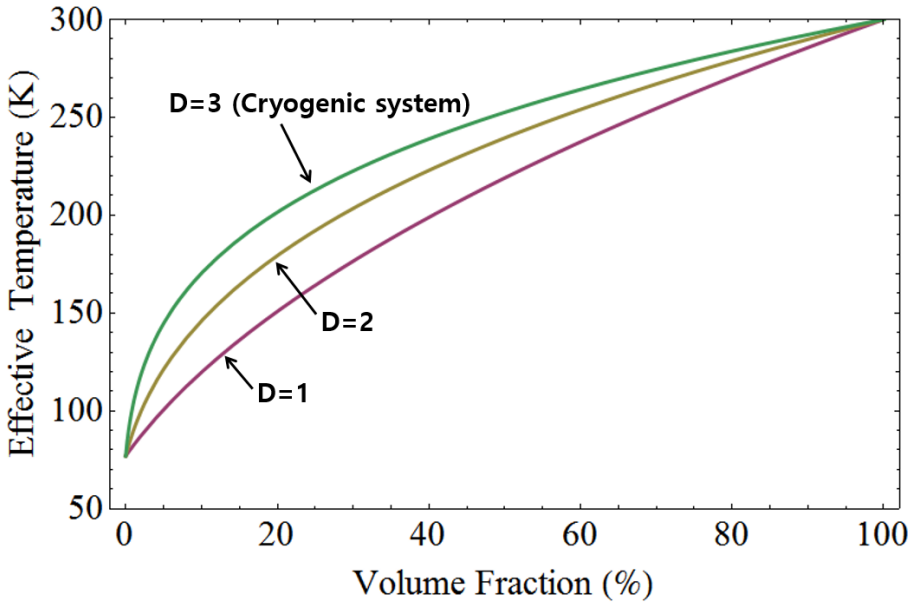


**Figure 6.** The effective temperature portrayed as a function of the volume ratio for liquid nitrogen and room temperature. Specifically, the effective temperature is depicted with respect to the volume ratio of the 300 K volume to the 77 K volume. Notably, the effective temperature demonstrates an increase with higher dimensions or increased volume ratios.

Coefficient of Performance (*COP*) is an important metric for cryogenic systems. The ideal Coefficient of Performance (*COP*) for a refrigeration cycle is given by the Carnot *COP*, which represents the maximum possible efficiency of a refrigeration system operating between two temperature reservoirs. The Carnot *COP* for a refrigeration cycle is defined as:

$$COP_{Carnot} = \frac{T_{cold}}{T_{hot} - T_{cold}}, \tag{34}$$

where $T_{cold}$ is the absolute temperature of the cold reservoir and $T_{hot}$ is the absolute temperature of the hot reservoir. The Carnot *COP* for a cryogenic system cooling from 300 K to 4.5 K is 0.0152. The Carnot *COP* for a cryogenic system cooling from 300 K to 2 K is 0.0067.

The generalized effective temperature can be applied to the *COP*. The *COP* for a refrigeration or cooling system can be expressed in terms of the effective temperatures of the hot and cold reservoirs:

$$COP_{refrigeration} = \frac{T_{eff,\ cold}}{T_{eff,hot} - T_{eff,cold}}, \tag{35}$$

where $T_{eff,cold}$ is the absolute effective temperature of the cold reservoir (refrigerated space), $T_{eff,hot}$ is the absolute effective temperature of the hot reservoir where heat is rejected. The *COP* of a refrigeration system increases as the temperature difference between the cold and hot reservoirs decreases. Therefore, the system performs better (higher *COP*) when the temperature difference is smaller.

The figure of merit (*FOM*) is defined as:

$$FOM = \frac{COP_{real}}{COP_{Carnot}}, \tag{36}$$

where $COP_{real}$ is the actual *COP* and $COP_{Carnot}$ represents the *COP* of an ideal Carnot cycle. The *FOM* is approximately 0.3 or 30% for a 4.5 K cooling cryogenic system having $COP_{real} = 0.045$, In contrast, the FOM is around 0.15 or 15% for a 2 K cooling cryogenic system with $COP_{real} = 0.001$ [26].

The effective temperature represents the global temperature concept of a body, which is particularly useful when the local temperature distribution across the body is non-uniform. When seeking to determine the overall temperature of the body, calculating the effective temperature becomes essential. This paper offers valuable insights into computing the effective temperature for both integer and fractional dimensions, providing a useful resource for obtaining the effective temperature of a body across various dimensional spaces. This effective temperature can also be applied to low-dimensional materials, including one-dimensional materials such as carbon nanotubes and two-dimensional materials such as graphene. Additionally, it can be applied to high-energy accelerator physics, including high-dimensional physics. This research provides valuable insights into understanding the effective temperature of cryogenic systems, offering potential applications and benefits in this field.

## 7. Conclusions

We have demonstrated the characteristics of the generalized effective temperature across both fractional and arbitrary dimensions. Additionally, we present the energy densities of blackbody radiation across one, two, three, and higher dimensions. The Maxwell–Boltzmann distribution is displayed for one, two, and three dimensions, with effective temperatures expressed for each dimension. The generalization of effective temperature for non-uniform temperature distributions in various dimensions, from one to high dimensions, is provided. Furthermore, we compute the effective temperature for cryogenic liquids, including liquid nitrogen and liquid helium, and express the effective temperature of linearly non-uniform temperature distributions as a function of arbitrary

dimension. We also illustrate the effective temperature for two different temperature distributions for liquid nitrogen and liquid helium in terms of arbitrary dimensions and volume fractions. The effective temperature is applied to the Coefficient of Performance (COP) in cryogenic systems. This generalized effective temperature can be useful for low-dimensional materials, including one-dimensional materials such as carbon nanotubes, and two-dimensional materials such as graphene, as well as for high-energy accelerator physics, including high-dimensional physics.

**Author Contributions:** H.K.: Conceptualization, investigation, writing—original draft, writing—review and editing. C.-S.P.: investigation, validation, writing—review and editing. All authors have read and agreed to the published version of the manuscript.

**Funding:** This research was supported by the National Research Foundation of Korea (NRF) and funded by the Ministry of Science and ICT under grant RS-2022-00214790.

**Data Availability Statement:** The data supporting this study's conclusions are available from the corresponding author upon reasonable request.

**Acknowledgments:** The authors thank the researchers who contributed to discussions on effective temperature at IRIS.

**Conflicts of Interest:** The authors declare that there are no conflicts of interest.

## References

1. Landsberg, P.T.; De Vos, A. The Stefan-Boltzmann constant in n-dimensional space. *J. Phys. A Math. Gen.* **1989**, *22*, 1073. [CrossRef]
2. Yu, S.J.; Youn, S.J.; Kim, H. Size effect of thermal radiation. *Phys. B* **2010**, *405*, 638. [CrossRef]
3. Kim, H.; Lim, S.C.; Lee, Y.H. Size effect of two-dimensional thermal radiation. *Phys. Letts. A* **2011**, *375*, 2661. [CrossRef]
4. Kim, H.; Youn, S.J.; Yu, S.J. Generalized Thermionic Emission for Arbitrary Dimension. *J. Kor. Phys. Soc.* **2010**, *56*, 554. [CrossRef]
5. Schulz, M.; Caldwell, L. Nonuniformity correction and correctability of infrared focal plane arrays. *Infrared. Phys. Technol.* **1995**, *36*, 763. [CrossRef]
6. Orzanowski, T.; Madura, H. Test and evaluation of reference-based nonuniformity correction methods for microbolometer infrared detectors. *Opto.-Electron. Rev.* **2010**, *18*, 91. [CrossRef]
7. Bao, X.; Webb, D.J.; Jackson, D.A. Combined distributed temperature and strain sensor based on Brillouin loss in an optical fiber. *Opt. Lett.* **1994**, *19*, 141. [CrossRef]
8. Ji, J.K.; Yoon, J.R.; Cho, K. Nonuniformity correction scheme for an infrared camera including the background effect due to camera temperature variation. *Opt. Eng.* **2000**, *39*, 936. [CrossRef]
9. Vollmerhausen, R.H. Representing the observer in electro-optical target acquisition models. *Opt. Eng.* **2009**, *48*, 0764019. [CrossRef]
10. Kim, H.; Han, M.S.; Perello, D.; Yun, M. Effective temperature of thermal radiation from non-uniform temperature distributions and nanoparticles. *Infrared. Phys. Technol.* **2013**, *60*, 7. [CrossRef]
11. Kim, H.; Park, C.S.; Han, M.S. Effective temperature of two-dimensional material for non-uniform temperature distribution. *Opt. Commun.* **2014**, *325*, 68. [CrossRef]
12. Coniglio, A.; Arcangelis, D.; Herrmann, H.J. Fractals and multifractals: Applications in physics. *Phys. A* **1989**, *157*, 21. [CrossRef]
13. Theiler, J. Estimating fractal dimension. *J. Opt. Soc. Am. A* **1990**, *7*, 1055. [CrossRef]
14. Keith, C.C.; Diane, M.S. Measuring the Fractal Dimension of Natural Surfaces Using a Robust Fractal Estimator. *Cartogr. Geogr. Inf. Syst.* **1991**, *18*, 37.
15. Draves, S.; Abraham, R.; Viotti, P.; Abraham, F.D.; Sprott, J.C. *International Journal of Bifurcation and Chaos*; World Scientific: Singapore, 2008; Volume 18, p. 1243.
16. Cervantes-De la Torre, F.; González-Trejo, J.I.; Real-Ramírez, C.A.; Hoyos-Reyes, L.F. Fractal dimension algorithms and their application to time series associated with natural phenomena. *J. Phys. Conf. Ser.* **2013**, *475*, 012002. [CrossRef]
17. Garg, A.; Agrawa, A.; Negi, A. A Review on Natural Phenomenon of Fractal Geometry. *Int. J. Comput. Appl.* **2014**, *86*, 1–7. [CrossRef]
18. Chen, Y.; Zhang, C.; Shi, M.; Peterson, G.P. Optimal surface fractal dimension for heat and fluid flow in microchannels. *App. Phys. Lett.* **2010**, *97*, 084101. [CrossRef]
19. Nam, S.T. Heat Capacity of Liquid Helium II in a Fractal Dimension. *J. Korean Phys. Soc.* **2004**, *44*, 464.
20. Kim, H.; Kim, W.; Park, G.T.; Shin, I.; Choi, S.; Jeon, D.O. Generalized thermal radiation from arbitrary fractional dimension. *Infrared. Phys. Technol.* **2014**, *67*, 600. [CrossRef]
21. Shahsafi, A.; Roney, P.; Zhoub, Y.; Zhang, Z.; Xiao, Y.; Wan, C.; Wambold, R.; Salman, J.; Yu, Z.; Li, J.; et al. Temperature-independent thermal radiation. *Proc. Natl. Acad. Sci. USA* **2019**, *116*, 26402. [CrossRef]

22. Sakai, H.; Cenni, E.; Enami, K.; Furuya, T.; Sawamura, M.; Shinoe, K.; Umemori, K. Field emission studies in vertical test and during cryomodule operation using precise X-ray mapping system. *Phys. Rev. Accel. Beams* **2019**, *22*, 022002. [CrossRef]
23. Tan, J. Field emission studies at Saclay and Orsay. *Part Accel.* **1996**, *53*, 1.
24. Vines, J.; Xie, Y.; Padamsee, H. Systematic Trends for the Medium Field Q-Slope. In Proceedings of the SRF2007, Beijing, China, 14–19 October 2007; TUP27. p. 178.
25. Weingarten, W.; Eichhorn, R. Field-dependent surface resistance for superconducting niobium accelerating cavities: The case of N doping. In Proceedings of the 17th International Conference on RF Superconductivity (SRF2015), Whistler, BC, Canada, 13–18 September 2015; MOPB010. p. 95.
26. Oonk, R.L.; Hustvedt, D.C. The Effect of Fluid Property Variations on the Performance of Cryogenic Helium Heat Exchangers. In *Advances in Cryogenic Engineering*; Fast, R.W., Ed.; Springer: Boston, MA, USA, 1986; Volume 31, pp. 415–422. [CrossRef]